Article

Molecular Drug Simulation and Experimental Validation of the CD36 Receptor Competitively Binding to Long-Chain Fatty Acids by 7-Ketocholesteryl-9-carboxynonanoate

Changzhen Fu,[||] Meng-Lin Xiang,[||] Shaolang Chen, Geng Dong, Zibo Liu, Chong-Bo Chen, Jiajian Liang, Yingjie Cao, Mingzhi Zhang,* and Qingping Liu*

Read Online

ACCESS | Metrics & More | Article Recommendations

ABSTRACT: Long-chain fatty acids (LCFAs) are one of the main energy-supplying substances in the body. LCFAs with different lengths and saturations may have contrasting biological effects that exacerbate or alleviate progress against a variety of systemic disorders of lipid metabolism in organisms. Nonalcoholic fatty liver disease is characterized by chronic inflammation and steatosis, mainly caused by the ectopic accumulation of lipids in the liver, especially LCFAs. CD36 is a scavenger receptor that recognizes and mediates the transmembrane absorption of LCFAs and is expressed in a variety of cells throughout the body. In previous studies, our group found that 7-ketocholesteryl-9-carboxynonanoate (oxLig-1) has the biological effect of targeting CD36 to inhibit oxidized low-density lipoprotein lipotoxicity-induced lipid

metabolism disorder; it has an ω-carboxyl physiologically active center and is structurally similar to LCFAs. However, the biological mechanism of oxLig-1 binding to CD36 and competing for binding to different types of LCFAs is still not clear. In this study, molecular docking and molecular dynamics simulation were utilized to simulate and analyze the binding activity between oxLig-1 and different types of LCFAs to CD36 and confirmed by the enzyme-linked immunosorbent assay (ELISA) method. Absorption, distribution, metabolism, excretion, and toxicity (ADMET) platform was applied to predict the drug-forming properties of oxLig-1, and HepG2 cells model of oleic acid and nonalcoholic fatty liver disease (NAFLD) model mice were validated to verify the biological protection of oxLig-1 on lipid lowering. The results showed that there was a co-binding site of LCFAs and oxLig-1 on CD36, and the binding driving forces were mainly hydrogen bonding and hydrophobic interactions. The binding abilities of polyunsaturated LCFAs, oxLig-1, monounsaturated LCFAs, and saturated LCFAs to CD36 showed a decreasing trend in this order. There was a similar decreasing trend in the stability of the molecular dynamics simulation. ELISA results similarly confirmed that the binding activity of oxLig-1 to CD36 was significantly higher than that of typical monounsaturated and saturated LCFAs. ADMET prediction results indicated that oxLig-1 had a good drug-forming property. HepG2 cells model of oleic acid and NAFLD model mice study results demonstrated the favorable lipid-lowering biological effects of oxLig-1. Therefore, oxLig-1 may have a protective effect by targeting CD36 to inhibit the excessive influx and deposition of lipotoxicity monounsaturated LCFAs and saturated LCFAs in hepatocytes.
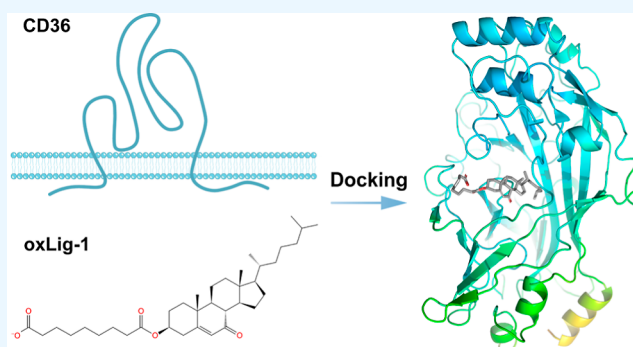
1. INTRODUCTION

1.1. Nonalcoholic Fatty Liver Disease. Nonalcoholic fatty liver disease (NAFLD) is considered the most common liver disease in the world and affects 30% of the general population.[1] NAFLD is also one of the most common causes of hepatocellular carcinoma.[2−4] A high-fat diet causes an increased incidence of metabolic disorders, and NAFLD is one of the markers of high-fat diet-induced metabolic syndrome.[5] Although its disease burden continues to increase, diagnosis and treatment options are still very limited. For NAFLD, liver protection and symptomatic treatments are usually used in the course of the disease, but treatments to prevent and improve

lipid deposition in the body by regulating the body's lipid intake with drugs are still limited.[6,7] To date, several proteins that promote fatty acid uptake in vivo have been reported, including CD36, Caveolin-1, fatty acid transport proteins (FATPs), fatty

acid-binding proteins (FABPs), and G protein-coupled fatty acid receptors (FFARs), and so forth, of which CD36 plays a major role in the absorption of fatty acids, especially LCFAs.[8,9]

1.2. CD36 Transmembrane Protein Receptor. CD36 is a scavenger receptor involved in the fundamental processes such as fatty acid metabolism, natural immunity, and angiogenesis and is present in a variety of cells in the body, including platelets, immune cells, adipocytes, myocytes, enterocytes, enteroendocrine cells, retinal pigment epithelial cells, mammary epithelial cells, and microvascular endothelial cells.[10] CD36 is a secondary transmembrane glycoprotein, consisting of 472 aa, with a relative molecular weight of about 88 kDa, and C and N terminals located intracellularly (Figure 1). Post-translational
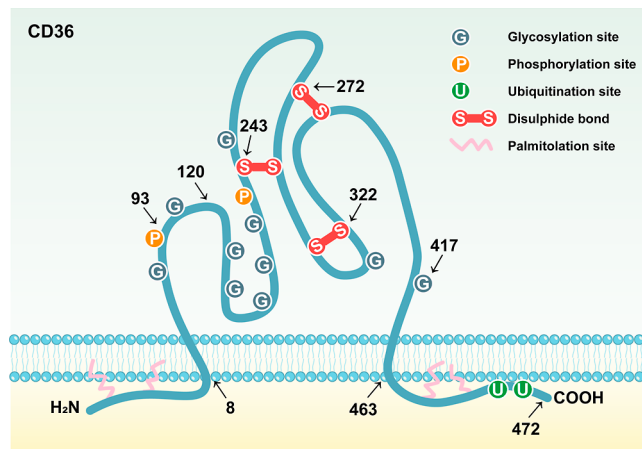

Figure 1. CD36 molecular transmembrane diagram (reproduced and adapted with permission from Glatz et al.,[17] Copyright 2018 by the American Society for Biochemistry and Molecular Biology, Inc.).

modifications of the protein (including glycosylation, palmitoylation, ubiquitination, and phosphorylation) have been found to affect the function of CD36 in fatty acid uptake and signal transduction.[11]

In 1977, CD36 was first described as "glycoprotein IV (GP IIIb or GP IV)", the fourth major band (a molecular mass of approximately 88 kDa) observed on sodium dodecyl sulfate—polyacrylamide gel electrophoresis of platelet membranes.[12] In 1984, it was found to be the same as the antigen recognized by the monoclonal antibody OKM5, a marker of monocytes and macrophages, so it was named a cluster of differentiation 36, or CD36.[13] In 1993, Abumrad et al. discovered the role of CD36 in the cellular uptake of LCFAs,[14] and in the same year, a study by Endemann et al. identified that it is also a receptor for oxidized low-density lipoprotein.[15] The human CD36 crystal structure (PDB ID: 5LGD) was resolved in 2016.[16] CD36 interacts with lipoprotein particles to promote the absorption of LCFAs.

1.3. Long-Chain Fatty Acids. As one of the basic nutrients of the body, fatty acids are involved in various important life processes, such as energy storage and biofilm synthesis.[18,19] Fatty acids are monocarboxylic acids, which are divided into short-chain (2C−4C), medium-chain (6C−12C), and long-chain (14C−24C) fatty acids according to the number of carbon atoms[20] and further divided into saturated and unsaturated fatty acids according to the presence or absence of double bonds on the carbon chain.[21] Mammals can synthesize saturated fatty acids and monounsaturated fatty acids, but not polyunsaturated fatty acids. Essential fatty acids are essential for humans but cannot be synthesized by humans and need to be obtained from

food, including linoleic acid (C18:2) and α-linolenic acid (C18:3). In the human body, these fatty acids participate in the production of arachidonic acid (C20:4), eicosapentaenoic acid (C20:5), and docosahexaenoic acid (DHA, C22:6) and play a key role in regulating homeostasis.[22] The main dietary LCFAs include myristic acid (C14:0), palmitic acid (C16:0), stearic acid (C18:0), and oleic acid (C18:1), among others.[23]

Excessive intake of saturated LCFAs may lead to lipid metabolism disorders, which may cause various diseases, including NAFLD. Epidemiological studies have pointed out that a high-fat diet rich in saturated LCFAs causes multiple organ inflammation.[24] Saturated fatty acid-mediated cell death-induced lipotoxicity plays an important role in the pathogenesis of NAFLD.[25] Most polyunsaturated LCFAs, especially ω-3 polyunsaturated LCFAs, play an important role in the growth and development and in preventing the accumulation of cholesterol and fat on the arterial wall. The ω-3 polyunsaturated LCFAs can change the composition of the plasma membrane and regulate gene expression and certain cell signaling pathways, playing an important protective role in many chronic diseases, including cardiovascular disease, type 2 diabetes, and even cancer,[26,27] and may help reduce liver triglycerides (DHA may be more effective than eicosapentaenoic acid).[28] Studies have shown that approximately 59% of liver triglycerides in NAFLD patients is derived from serum nonesterified fatty acid transmembrane transport, 26% from de novo lipogenesis, and 15% from dietary sources.[29] Of these fatty acids, palmitic acid (C16:0), stearic acid (C18:0), oleic acid (C18:1), linoleic acid (C18:2), arachidonic acid (C20:4), and DHA (C22:6) are most abundant in liver tissues and are metabolically disordered in the liver tissue of NAFLD mouse models.[30,31] At present, there is still no effective drug for the treatment of lipid metabolism disorders caused by excessive intake of saturated LCFAs and monounsaturated LCFAs.

1.4. 7-Ketocholesteryl-9-carboxynonanoate (oxLig-1). OxLig-1, the chemical name is 7-ketocholesteryl-9-carboxyno-nanoate. It is a new compound isolated, purified, and chemically synthesized from oxLDL by our group in 2001 Pubchem (CID: 101135439); the first study showed that oxLig-1 was a key epitope ligand that mediates the interaction between oxLDL and serum glycoprotein β2-GPI in autoimmune atherosclerosis.[32,33] Further studies revealed that as an epitope structure of oxLDL, oxLig-1 can specifically trigger the CD36-dependent signaling pathway to inhibit oxLDL-induced lipotoxic accumulation via JNK/ABCA1 and PPAR/ABCA1 signaling pathways.[34,35] The surface plasmon resonance (SPR) was applied and confirmed that the binding between oxLig-1 and CD36 with high-affinity, and the ω-carboxyl group of oxLig-1 was the key to maintain the binding stability of the both.[36]

In terms of chemical structure, LCFAs share the ω-carboxyl group with oxLig-1 and the other end is hydrophobic hydrocarbon chains and cholesterol cores. We hypothesized that oxLig-1 might have the effect of competing with LCFAs to bind to CD36 receptor, thus inhibiting the transmembrane uptake of LCFAs. As in silico methodologies have demonstrated efficiency in describing the interactions of complex,[37,38] molecular docking was suitable for depicting the interaction and binding affinity of protein−ligand,[39,40] molecular dynamics (MD) simulation was an approach to analyze the dynamic stability of the complex,[39,41] and the molecular mechanics-generalized Born surface area (MM/GBSA) was employed to calculate the binding energy between the molecules.[42−44] Thus, to assess this hypothesis and further extend the results, the

current study employed a variety of simulation tools to investigate the binding effect of oxLig-1 competing with LCFAs for CD36, confirmed the binding activity of oxLig-1 and LCFAs to CD36 by enzyme-linked immunosorbent assay (ELISA), assessed the drug-forming properties of oxLig-1 by absorption, distribution, metabolism, excretion, and toxicity (ADMET) prediction, and verified the lipid-lowering effect of oxLig-1 by HepG2 cells model of oleic acid and NAFLD model mice experiments.

In general, current researches on CD36 function have evolved from lipid metabolism diseases[45,46] to ophthalmic diseases,[47] tumors,[48] and so forth. This study aimed to establish a molecular model of CD36 binding to oxLig-1 and LCFAs and conducted preliminary in vivo and in vitro experimental studies to validate the proposed model. The insights gained from this study have valuable implications for the development of drugs that target receptor proteins.

2. MATERIALS AND METHODS

2.1. Molecular Docking and Molecular Dynamics Simulation Analysis Platform. Schrödinger Suites (Schrödinger, Inc., New York, NY, USA, version 12.6) were applied for molecular docking, Prime/MMGBSA calculating, and MD simulation.[49] CD36 protein crystallographic structures were obtained from the PDB database (https://www.rcsb.org/, PDB ID: 5LGD).[16] Ten ligands were used in the study, and their molecular structures were obtained from the PubChem database (https://pubchem.ncbi.nlm.nih.gov/). Nine LCFAs of different chain lengths and saturation were used, including stearic acid (SA, C18:0), palmitic acid (PA, C16:0), oleic acid (OA, C18:1), palmitoleic acid (POA, C16:1), linoleic acid (LOA, C18:2), arachidonic acid (ARA, C20:4), eicosapentaenoic acid (EPA, C20:5), docosahexaenoic acid (DHA, C22:6), neuronic acid (NA, C24:1), and oxLig-1 (PubChem CID 101135439).

2.2. Molecular Docking. Simulations were performed using the Schrödinger software Maestro 12.6 glide ligand docking module. Pymol was used for the visualization of protein–ligand complex structural interactions for mapping. Schrödinger software was applied to normalize the preprocessing of the receptor protein (CD36) and ligand small molecules (LCFAs, oxLig-1) to define the ligand binding sites of the proteins (Grid1 center coordinates: X-42.74 Y-26.50 Z-16.17; Grid2 center coordinates: X-41.38 Y-32.42 Z-35.02; Grid3 center coordinates: X-45.14 Y-33.64 Z-22.02). Grid1 and Grid2 are known long-chain fatty acid binding sites in the protein crystallographic structure,[16] and in this study, Schrödinger sitemap tool was applied to identify top-ranked potential receptor binding sites (all atoms in the workspace constitute the receptor); using more restrictive definition of hydrophobicity, the standardized Grid3 was generated. Before docking, the protein structure was prepared using the "Protein Preparation Wizard" protocol of Schrödinger. Semi-flexible docking was also performed, specifying the receptor protein CD36 as rigid and the ligand small molecule as flexible. Binding energy calculations were performed using the Prime/MM-GBSA module of Schrödinger for all docked compounds.

2.3. Molecular Dynamics Simulation. MD simulation was performed using the Schrödinger software Maestro Desmond MD module. The simulation system of the complex was established using the system builder tool of the Schrödinger Desmond module. The complexes were situated in a cubic water box with 10 Å buffer distance, and simple point charge (SPC) was selected in the solvent model, which allowed for the

conversion of the periodic physical problems into a periodic unit process and introduced periodic boundary conditions to eliminate the influence of boundary effects on small-scale simulation systems.[50] NaCl was added as a solvent molecule, with a salt concentration of 0.15 M, and additional Na^+/Cl^- ions were added into the simulation system to maintain electrical neutrality. Long-range electrostatic interactions were calculated using the particle mesh Ewald,[51] while a shear radius of 9.0 Å was applied for short-range electrostatics and van der Waals interactions.[52] All atom force field OPLS_2005 was adopted. Afterward, two restrained short simulations in NVT and NPT ensembles were performed using the default protocol of Desmond in Maestro to relax the minimized systems. The temperature and pressure during the simulation were set to 300 K and 1 atm maintained by the Nosè—Hoover chain thermostat and Martyna—Tobiase—Klein barostat methods, respectively. Finally, a 120 ns long MD run was performed in the NPT ensemble.[40,52]

2.4. Enzyme-Linked Immunosorbent Assay. OxLig-1 was synthesized and identified by our research group according to previous methods.[33,53] Oxlig-1, oleic acid (O1008, Sigma), palmitoleic acid (P9417, Sigma), stearic acid (S4751, Sigma), and palmitic acid (P0500, Sigma) were dissolved in anhydrous ethanol to a final concentration of 50 μg/mL and coated into 96-well polystyrene plates (50 μL/well) by ethanol evaporation. The plates were blocked with PBS containing 1% gelatin for 1 h. Then, recombinant human CD36 protein with His tag (50 μg/mL, 10752H08H50, Invitrogen), anti-His antibody (1:1000, ZSGB-BIO, China), and HRP-labeled secondary antibody (1:1000, ZSGB-BIO, China) was added and incubated for 1 h, Finally, the color was developed with *o*-phenylenediamine buffer containing H_2O_2 and terminated by 2 N H_2SO_4. Absorbance was measured at 492 nm. In each step, the wells were extensively washed with PBS containing 0.05% Tween-20.

2.5. ADMET Prediction. The computer prediction of ADMET is an important part of drug research and development. At the early stage of drug discovery, the evaluation of pharmacokinetic characteristics is the key to guiding the optimization of hit-to-lead and lead optimization. The ADMET prediction was performed by ADMETlab 2.0 (Xiangya School of Pharmaceutical Sciences, Central South University),[54] and toxicity analysis was calculated with Protox-II (Hasselgren and Myatt 2018).[55]

2.6. HepG2 Cells Culture. HepG2 cells were purchased from the China Center for Type Culture Collection (CCTCC), Wuhan, China, and cultured in a high-glucose DMEM (11995065, GIBCO) complete medium containing 10% fetal bovine serum (10270-106, GIBCO) and 1% penicillin–streptomycin at 37 °C and 5% CO_2. The collected cells were inoculated into a six-cell culture plate at 1×10^6 cells/well. After 24 h, HepG2 cells were incubated with oleic acid and a combination of oxLig-1. After 24 h, the collected cells were fixed with 4% paraformaldehyde, stained with oil red O, and photographed for observation. Intracellular lipid changes were analyzed by ImageJ software.

2.7. Animals Experiment. Male C57BL/6 mice (5—6 weeks of age) were purchased from Beijing Vital River Laboratory Animal Technology Co., Ltd.; the high-fat diet (MD12032) and control diet (MD12031) for mice were purchased from Jiangsu Madison Biological Medicine Co., Ltd. C57BL/6 mice were raised at a constant temperature of 25 °C with a 12:12 h light cycle in a standard specific pathogen-free (SPF) grade environment. After one week of adaptive feeding,
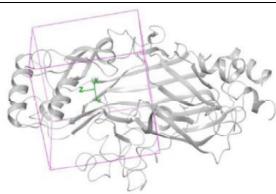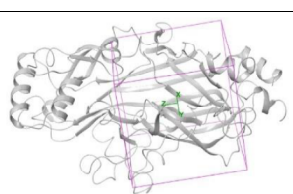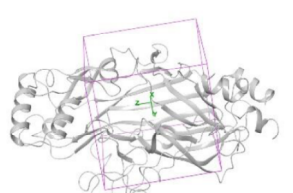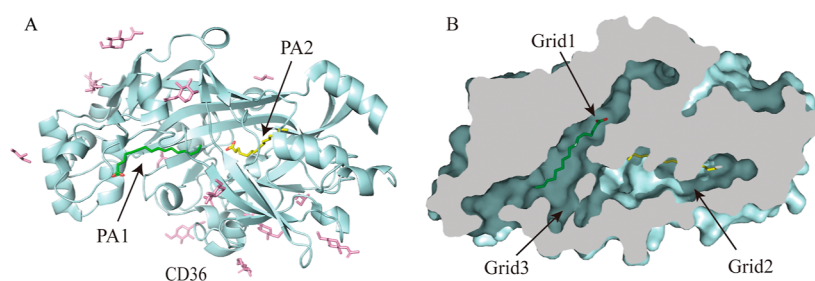
Figure 2. (A) Molecular structure of CD36 (PDB ID: 5LGD) is shown in the cartoon form. The structure of CD36 shown in light blue. The N-linked glycosylation sites and associated sugars are pink, while two palmitic acids are shown as green and yellow sticks, designated as PA1 (green) in Grid1 and PA2 (yellow) in Grid2, respectively. (B) Cross section of the surface structure shows cavities containing two palmitic acid ligands, and the "luminal channel" converged by the termini of Grid1 and Grid2 which designated as Grid3 (black arrowheads).

Table 1. Docking Score of Ligands Binding in Three Grids of CD36

Grid	ligand name	C∶C=C	docking score	central coordinate
Grid1	Nervonic acid	24∶1	-6.464	
	Docosahexaenoic acid	22∶6	-6.318	
	Arachidonic acid	20∶4	-6.173	
	Eicosapentaenoic acid	20∶5	-6.058	
	Stearic acid	18∶0	-3.545	
	Oleic acid	18∶1	-3.523	
	Linoleic acid	18∶2	-3.389	
	Palmitoleic acid	16∶1	-2.925	
	Palmitic acid	16∶0	-2.641	X-42.74 Y-26.50 Z35.02
	oxLig-1	/	/	
Grid2	Nervonic acid	24∶1	-7.286	
	Docosahexaenoic acid	22∶6	-6.802	
	Eicosapentaenoic acid	20∶5	-6.766	
	Arachidonic acid	20∶4	-5.846	
	Palmitoleic acid	16∶1	-2.566	
	Stearic acid	18∶0	-2.494	
	Linoleic acid	18∶2	-2.375	
	Palmitic acid	16∶0	-2.105	
	Oleic acid	18∶1	-1.896	X-41.38 Y-32.42 Z35.02
	oxLig-1	/	/	
Grid3	Nervonic acid	24∶1	-7.985	
	Docosahexaenoic acid	22∶6	-6.138	
	Eicosapentaenoic acid	20∶5	-5.449	
	Arachidonic acid	20∶4	-6.37	
	oxLig-1	/	-5.357	
	Oleic acid	18∶1	-2.471	
	Linoleic acid	18∶2	-2.393	
	Palmitoleic acid	16∶1	-1.708	
	Stearic acid	18∶0	-1.629	X-45.14 Y-33.64 Z22.02
	Palmitic acid	16∶0	-1.208	

mice were randomly divided into a high-fat group (HFD), oxLig-1 intervention group (HFDO), and control group (CON), with 10 mice in each group. The mice in the HFDO and HFD groups were fed with a high-fat diet (45% fat kcal, contains oleic acid 73.5 g/kg, palmitoleic acid 3.4 g/kg, stearic acid 26.5 g/kg, palmitic acid 47.1 g/kg, and linoleic acid 32.4 g/kg, etc., the total LCFA content was 190.6 g/kg), and the CON group was fed with a control diet (10% fat kcal, contains oleic acid 13.4 g/kg, palmitoleic acid 0.4 g/kg, stearic acid 3.8 g/kg, palmitic acid 7.9 g/kg, and linoleic acid 14.6 g/kg, etc., the total

LCFAs content was 42.2 g/kg) for 14 weeks. In addition, in the last 4 weeks of the feeding period, the HFDO group was administered oxLig-1 intragastrically at 10 mg/kg/day and the vehicle (0.5% sodium carboxymethyl cellulose [CMC-Na] dispersion) at the same dose was intragastrically administered to the HFD group and CON group. The mice were sacrificed by cervical dislocation. The liver was fixed in 4% paraformaldehyde, and paraffin sections (4 μm) were prepared and subjected to hematoxylin−eosin (HE) staining. All animal experiments were conducted in accordance with accepted standards for animal

Table 2. Prime MM-GBSA Energies (kcal/mol) for Ligands Binding to grid3 of CD36

ligand	ΔG bind	ΔG coulomb	ΔG covalent	ΔG Hbond	ΔG lipo	ΔG solv GB	ΔG vdW
nervonic acid	−109.23	−7.8	7.06	−0.66	−85.75	38.99	−61.06
oleic acid	−76.51	0.38	2.72	−2.74	−58.87	29.58	−47.58
stearic acid	−73.72	−2.97	6.53	−6.82	−56.76	35.3	−48.99
linoleic acid	−65.37	−2.41	−2.37	−2.82	−44.57	30.56	−43.78
arachidonic acid	−64.93	−4.04	0.32	−6.63	−44.86	33.16	−42.88
palmitoleic acid	−63.58	−4.29	5.27	−6.72	−48.49	30.04	−39.4
oxLig-1	−56.83	−17.03	0.47	−2.38	−35.73	34.99	−37.14
palmitic acid	−51.2	−4.27	7.17	−5.87	−49.14	30.62	−29.71
docosahexaenoic acid	−46.8	3.19	2.27	−2.25	−47.76	35.75	−38
eicosapentaenoic acid	−35.57	6.15	9.22	−3.56	−47.98	31.41	−30.81

protection and welfare and approved by the Animal Ethics Committee of Joint Shantou International Eye Center of Shantou University and The Chinese University of Hong Kong.

2.8. Statistical Analysis. The results are presented as mean ± SD. Statistical analysis was performed using Student's *t*-test. *P* < 0.05 was considered statistically significant.

3. RESULTS

3.1. Molecular Docking. *3.1.1. Binding Pockets of CD36.* We obtained the spatial locations of the two known binding pockets Grid1 and Grid2 from the resolved CD36 crystallographic structure. Based on the positions and the characteristics of the ability to bind LCFAs of Grid1 and Grid2, it was found that their termini converge into a large "luminal channel" mainly composed of hydrophobic amino acid arrangement. Thus, we obtained another potential protein binding pocket at this position through calculation and defined it as Grid3 (Figure 2).

3.1.2. Docking Score. Molecular docking can be used to analyze the binding mode, characteristics, and affinity of protein−ligand binding. The nine mentioned LCFAs were found to bind to three potential sites (referred as Grid1−3) on the CD36 protein structure. It is notable that oxLig-1 specifically bound to Grid3. We calculated the docking scores of CD36 and the ligands, the ratio of the number of carbon atoms to the carbon−carbon double bond, as well the positions of the three grids for CD36 binding to the ligands and their central coordinates, as shown in Table 1. The binding energies of CD36 to the LCFAs and oxLig-1 according to the docking score functions were all negative, indicating the ligand and protein bound spontaneously. A low score generally meant a better binding capacity. The binding ability of the different small molecules to the receptor differed. According to the docking score, the polyunsaturated LCFAs were preliminarily predicted to have good binding abilities in all three docking pockets. The binding abilities of polyunsaturated LCFAs, oxLig-1, mono-unsaturated LCFAs, and saturated LCFAs to Grid3 of CD36 decreased in this order.

3.1.3. MM-GBSA. To obtain further accuracy in our protocol, the MM-GBSA of the docked protein−ligand complexes was calculated to assess the contribution of the different energy terms in the binding interaction. Table 2 displays the calculated ΔG bind values for the various energy components of the ligands bound to CD36 Grid3. Inspection of the free energy components in this table shows that for all compounds, lipophilic and van der Waals energies (ΔG Lipo and ΔG vdW) contribute the most to the ligand binding energy.

3.1.4. Binding Mechanism. In this study, we found that the binding of LCFAs and oxLig-1 to the CD36 protein was formed by amino acids on the protein surface recognizing the carboxy-terminal portion of the ligand, which was due to hydrophobic interactions, and then entered the intramolecular cavity from the protein surface, based on the spatial characteristics. After the ligand being entered the protein binding pocket, the carboxy-terminal portion of the ligand formed hydrogen bonds and/or salt bridges with nearby amino acid residues. Notably, residues 96R, 100K, and 385 commonly formed interactions with LCFAs, in addition, 58G,116Q, and 269S interacted with some ligands through hydrogen bonds were also observed. The main amino acids interacted with oxLig-1 were 231K and 238Y, as shown in Figure 3.

3.2. Molecular Dynamics Simulation. *3.2.1. Protein−Ligand Root-Mean-Square Displacement (Protein−Ligand rmsd).* The protein and ligand atomic weight root-mean-square displacement (protein−ligand rmsd) is a common indicator for evaluating the difference between predicted and crystallographic orientations in the rmsd of heavy atoms.[56] The average displacement change of the atoms relative to the reference frame that can be used to measure a particular frame is calculated for all frames in the trajectory. Using the first frame as reference, it is considered as time $t = 0$; r' is the position of the selected atom in the *x*th frame after superimposition on the reference frame, where the *x*th frame is recorded at time t.

Figure 4 shows the rmsd evolution of a protein on the left *y*-axis. All protein frames were first aligned on the reference frame backbone, and then the rmsd was calculated based on the atomic selection. Monitoring the rmsd of a protein provides insight into its structural conformation throughout the simulation. The rmsd analysis indicates whether the simulation has equilibrated and fluctuates at the end of the simulation around a thermally averaged structure. For small spherical proteins, a variation of 1−3 Å is perfectly acceptable. When the rmsd value stabilizes around a fixed value, the simulation reaches convergent equilibrium. The right *y*-axis shows the variation in the rmsd of the ligand, indicating how stable the ligand is relative to the protein and its binding pocket. "Lig fit Prot" shows the ligand rmsd when the protein−ligand complex was first aligned on the protein backbone of the reference and then the rmsd of the ligand atom weight was measured. According to the docking score order, the polyunsaturated LCFAs DHA and OA, oxLig-1, and saturated LCFA PA were selected for the experiments and MD simulations were performed using the complexes formed by each of the above four molecules with CD36.

3.2.2. Root-Mean-Square Fluctuation. The root-mean-square fluctuation (RMSF) is a useful measure for assessing local changes along the protein chain. Peaks on the plot indicate areas of the protein that exhibit the highest fluctuations during the simulation. Protein residues that interact with the ligand are marked by vertical bars highlighted in green color.
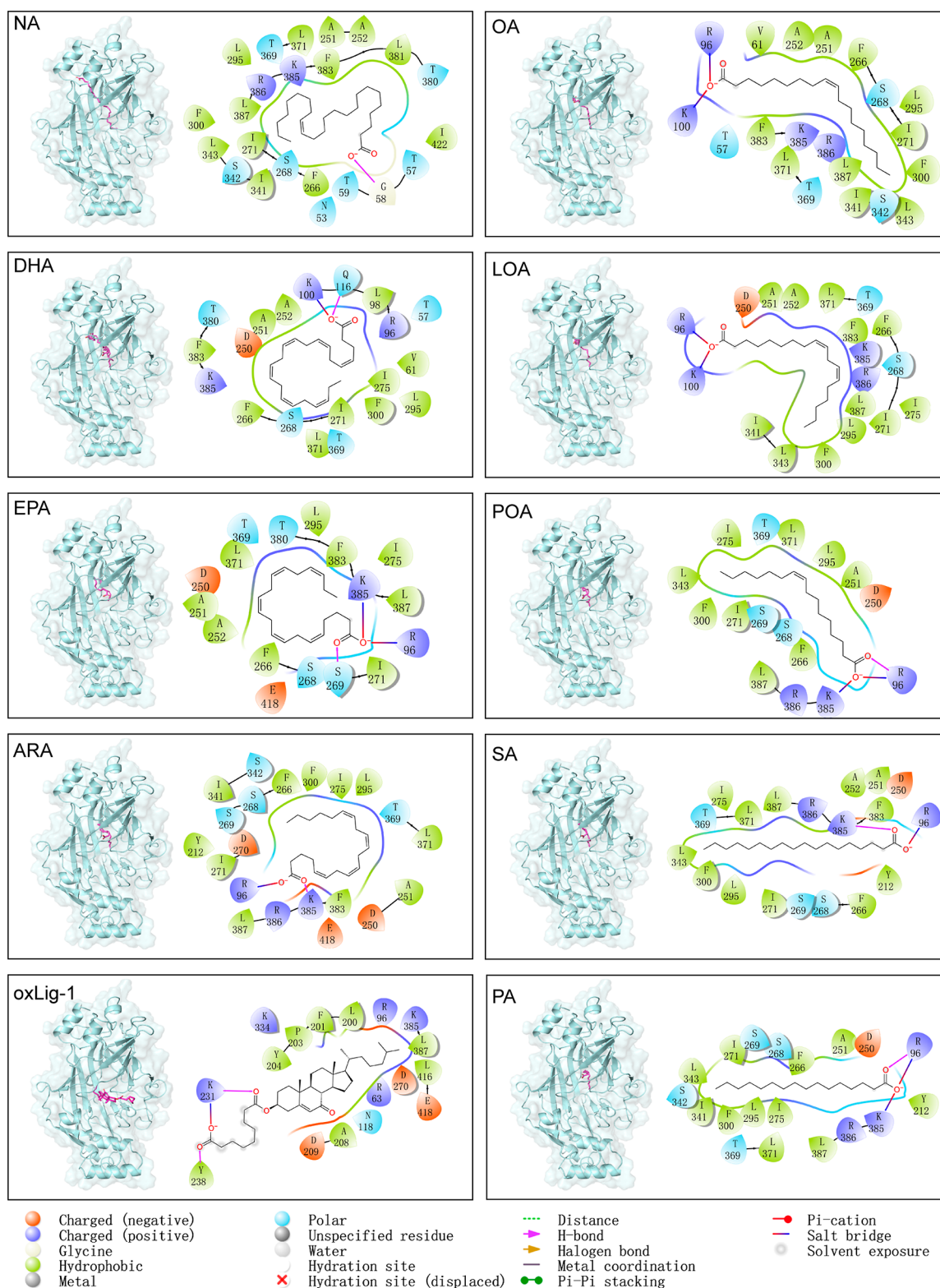
Figure 3. Binding patterns and interactions of 10 molecules with grid3 of CD36. The cartoon structure shows the binding position of the ligands in grid3 of CD36; the protein was shown in light blue while ligands in magenta. The images on the right offer detailed illustrations of the specific protein–ligand binding pattern and molecular interactions. The arrangement features of amino acid reveal that the binding pocket was mainly composed of hydrophobic amino acid residues.

Figure 5 displays the per-residue RMSFs of the protein. As shown, the overall fluctuation of protein alpha carbon is generally minimal; residues that interact with the ligands exhibit the least flexibility. Conversely, the remaining residues exhibit higher mobility. Residues with lower RMSF values are consistently found in similar regions across different complexes.

3.2.3. Protein–Ligand Interactions. Throughout the MD run, simulation interaction diagrams were generated to provide
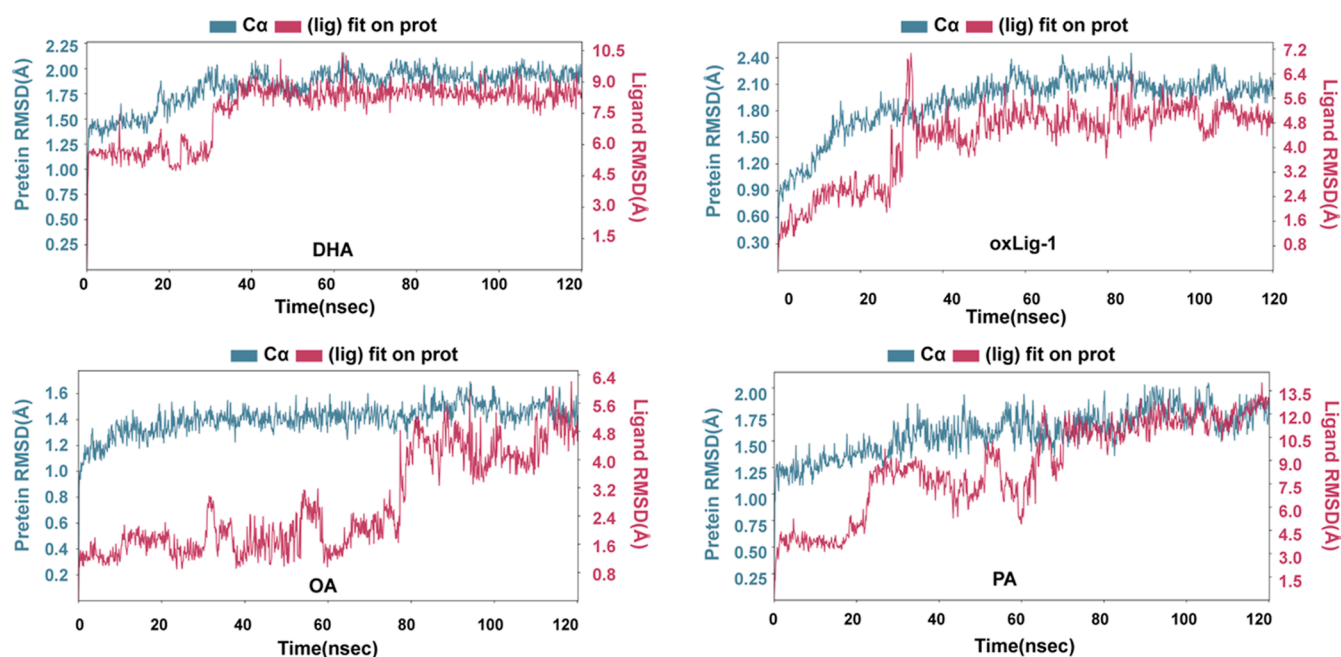
Figure 4. Changes in the atomic rmsd of the protein and ligand were recorded for 120 ns of the simulation run. After the four complexes were simulated and stabilized, the rmsd of the proteins all reached convergence around 2 Å with minimal fluctuations and it was assumed that the protein structures were stable during the simulations without major conformational changes. The rmsd of the complexes formed by DHA and oxLig-1 with CD36 began to converge after about 30 ns. The complexes of OA and CD36 show small fluctuations for the first 80 ns and a large positional fluctuation after 80 ns, after which they converged again steadily. The rmsd of the complexes formed by palmitic acid (PA) and CD36 began to converge after a large fluctuation at about 80 ns. For the rmsd of the small-molecule ligand after convergence, DHA fluctuated around 8 Å, oxLig-1 fluctuated around 5 Å, OA fluctuated around 5 Å, and PA fluctuated around 8 Å. Combined with the overall observation of MD motion trajectories, the complex formed by oxLig-1 and CD36 was considered more stable than the others.

insights into the interaction patterns between the four ligands and Grid3 of CD36. Protein–ligand interactions are categorized into four types: hydrogen bonds, hydrophobic, ionic, and water bridges. The stacked bar charts are normalized over the course of the trajectory; it should be noted that values over 1.0 are possible because some protein residues may make multiple contacts of same subtype with the ligand.

Figure 6 shows the interactions observed during the MD simulation. Ligands DHA, OA, and PA exhibited hydrogen bonding and water bridges with CD36, primarily through Lys385. Additionally, OA and PA demonstrated hydrogen bonds and water bridges with CD36, through Arg96. Hydrogen bonds and water bridges of ligand oxLig-1 with Asn108, Ala208, Lys231, Lys233, Tyr238, Lys334, and Arg337 were observed. Hydrophobic interactions were found to play a crucial role in the binding of all the selected ligands.

3.3. Analysis of oxLig-1 and LCFAs Binding Activity to CD36 by ELISA. To verify the molecular simulation results, monounsaturated LCFAs (oleic acid and palmitoleic acid) and saturated LCFAs (stearic acid and palmitic acid) and oxLig-1 were selected and their binding activities with CD36 were analyzed by ELISA. As shown in Figure 7, oxLig-1 specifically binds to CD36 with high affinity and the binding activities of oxLig-1 and CD36 were significantly higher than those of the other four LCFAs ($P < 0.01$). Based on the above results, it was suggested that oxLig-1 could inhibit the uptake of the above LCFAs by competitively bind to CD36.

3.4. ADMET Prediction. ADMET predictions indicated that the caco-2 (a model cell for evaluating drug absorption[57]) permeability of compound oxLig-1 was predicted to be −4.942 (optimum: higher than −5.15). The distribution was found to be 97.66% for plasma protein binding, and the volume

distribution was 0.852 L/kg (optimum: 0.04−20 L/kg), which is within the optimal range. In terms of metabolism, oxLig-1 did not inhibit most cytochromes. The excretion was predicted to have a clearance of 7.025 mL/min/kg, which is a moderate rate. The drug-induced liver injury (DILI) toxicity score was 0.028, which was a low DILI risk drug. The predicted value for oral acute toxicity in rats was 0.014 (where 0 indicates low toxicity and 1 indicates high toxicity), which is in the low toxicity range (Figure 8). Upon examination, these basic parameters were within their standard ranges and the predictions indicated that oxLig-1 is suitable for further development as a lead compound.

3.5. OxLig-1 Reduces Deposition of Cellular Lipids. To confirm the potential effect of oxLig-1 targeting CD36 to reduce LCFA-induced lipid deposition, in vitro, HepG2 cells were co-incubated with 0.5 mM oleic acid (OA group) and oleic acid combined with 20 μg/mL oxLig-1 (OAOL group) for 24 h. Oil red O staining showed that incubation with OA alone resulted in a significant increase in intracellular lipid deposition (Figure 9, OA), while co-incubation with oxLig-1 significantly decreased intracellular lipid deposition compared to incubation with OA alone (Figure 9, OAOL). Quantitative ImageJ analysis showed that the area of intracellular lipid deposition was significantly reduced by 83.1% ($p < 0.01$) in the OAOL group, indicating that oxLig-1 was able to significantly reduce oleic acid-induced intracellular lipid deposition. In vivo, liver HE staining of male C57BL/6 mice after high-fat and oxLig-1 gavage interventions showed that high-fat feeding led to the formation of a large number of lipid vacuoles in the liver of C57BL/6 mice (Figure 9, HFD), which were significantly reduced after oxLig-1 gavage intervention (Figure 9, HFDO). ImageJ quantitative analysis showed that the area of lipid vacuoles in the liver was significantly reduced by 83.9% ($P < 0.01$) in the OAOL
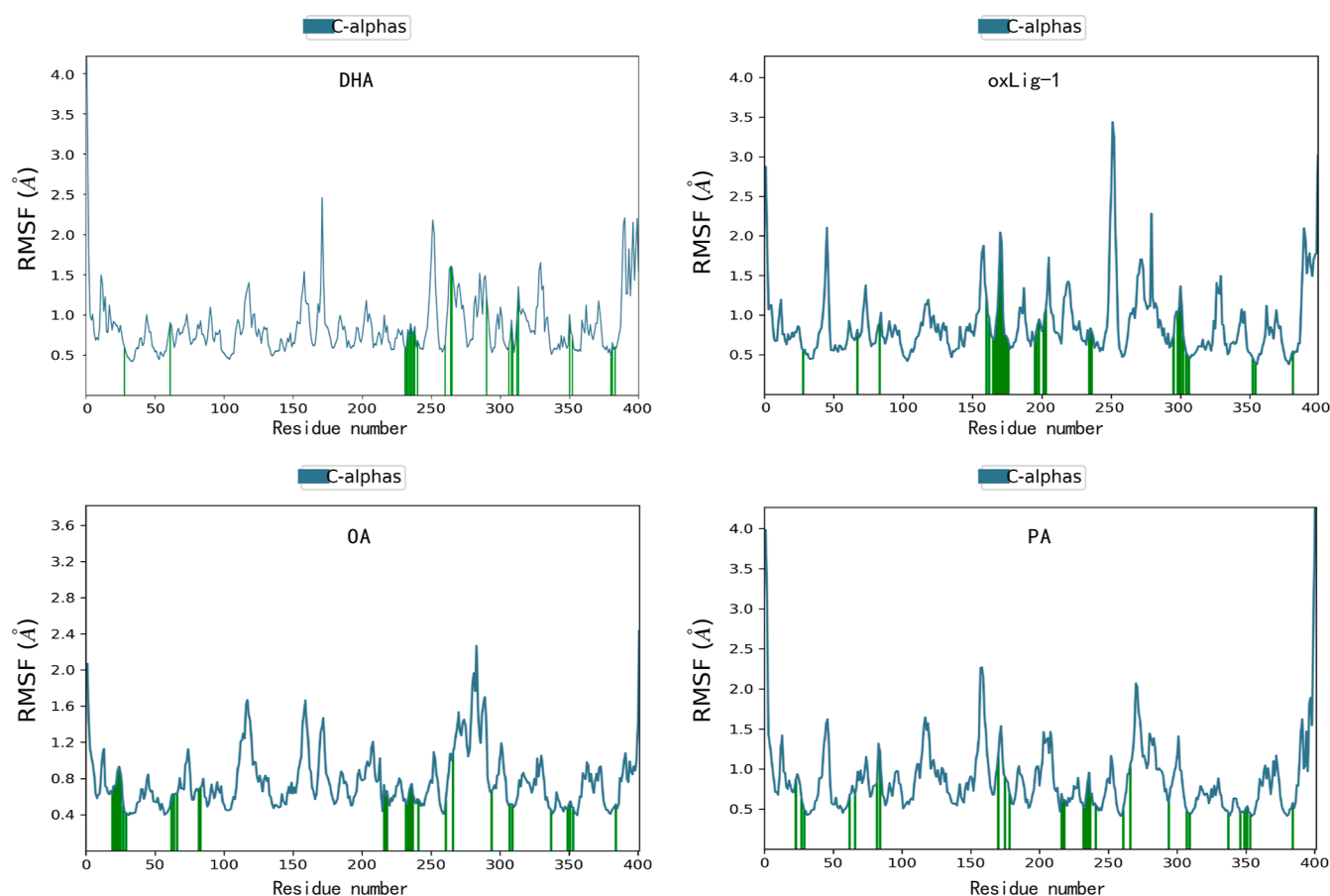
Figure 5. RMSF of the complexes that CD36 grid3 bind to different ligands.

group. This indicates that oxLig-1 ameliorated high lipid-induced hepatic lipid deposition in mice.

4. DISCUSSION

In this study, we have illustrated the binding mechanism, affinity, and stability of CD36 receptor with LCFAs and oxLig-1 through molecular docking and MD simulation. The results showed a trend that the binding force of oxLig-1 with CD36 was higher than that of monounsaturated LCFAs and saturated LCFAs, but lower than that of polyunsaturated LCFAs. It indicated that oxLig-1 might inhibit the transport of monounsaturated LCFAs and saturated LCFAs, but not inhibit the uptake of polyunsaturated LCFAs. ELISA results helped corroborate this finding. The results also revealed that the ω-carboxyl group common to oxLig-1 and LCFAs is a key site for specific binding to CD36, and the hydrophobic core of oxLig-1 has an important auxiliary binding effect. ADMET prediction results showed that oxLig-1 had a good drug-forming property. And it has been verified that oxLig-1 has a good biological pharmacological effect of inhibiting fatty acids deposition in the treatment of oleic acid cell model and NAFLD model mice.

NAFLD is characterized by chronic inflammation and steatosis, mainly caused by ectopic accumulation of lipids in the liver, especially LCFAs, which is widely prevalent due to generally high-fat diet.[58] CD36 is a scavenger receptor associated with fatty acid metabolism and is one of the major receptors for long-chain fatty acid uptake and is expressed in a variety of cells throughout the body.[9] LCFAs are involved in a variety of fundamental processes, with saturated LCFAs being one of the body's major energy donors, and some polyunsatu-

rated LCFAs are necessary for growth and developmental processes. Excessive intake of saturated LCFAs may cause a variety of systemic disorders of lipid metabolism, including NAFLD, while polyunsaturated LCFAs are often protective.[59] In the previous research, the mechanism of CD36 trans-membrane uptake of fatty acids focused on the upstream and downstream regulation pathways, and the physiological and pathological processes. However, the specific molecular binding mechanisms underlying the interaction between CD36 and LCFAs at the computational level have received relatively less attention. In addition, there is a lack of reported comparative studies on the competitive binding of oxidized sterols and LCFAs to CD36. Our previous studies found that oxLig-1, as the lipid epitope of oxLDL, could trigger the CD36-dependent signaling pathway and inhibit the accumulation of lipotoxicity induced by oxLDL,[34,35] and it could target CD36, the ω-carboxyl group of which was the key to maintain the binding stability of both.[36] OxLig-1 shares ω-carboxyl groups with LCFAs in the chemical structure,[32] in order to evaluate the effect that oxLig-1 may compete with LCFAs to bind CD36, thus inhibiting the transmembrane absorption of LCFAs, we investigated the binding mechanism of CD36 to LCFAs and oxLig-1 by docking simulations, binding free energy calculations, and MD simulations, and examined the inhibitory effect of oxLig-1 on the uptake of LCFAs, such as oleic acid, by cellular and animal experiments. Based on the results, it was hypothesized that oxLig-1 may act as a potential protective agent, using CD36 as a protein receptor target. This may play a role in regulating lipid uptake by inhibiting the binding uptake of saturated LCFAs by CD36 without inhibiting unsaturated
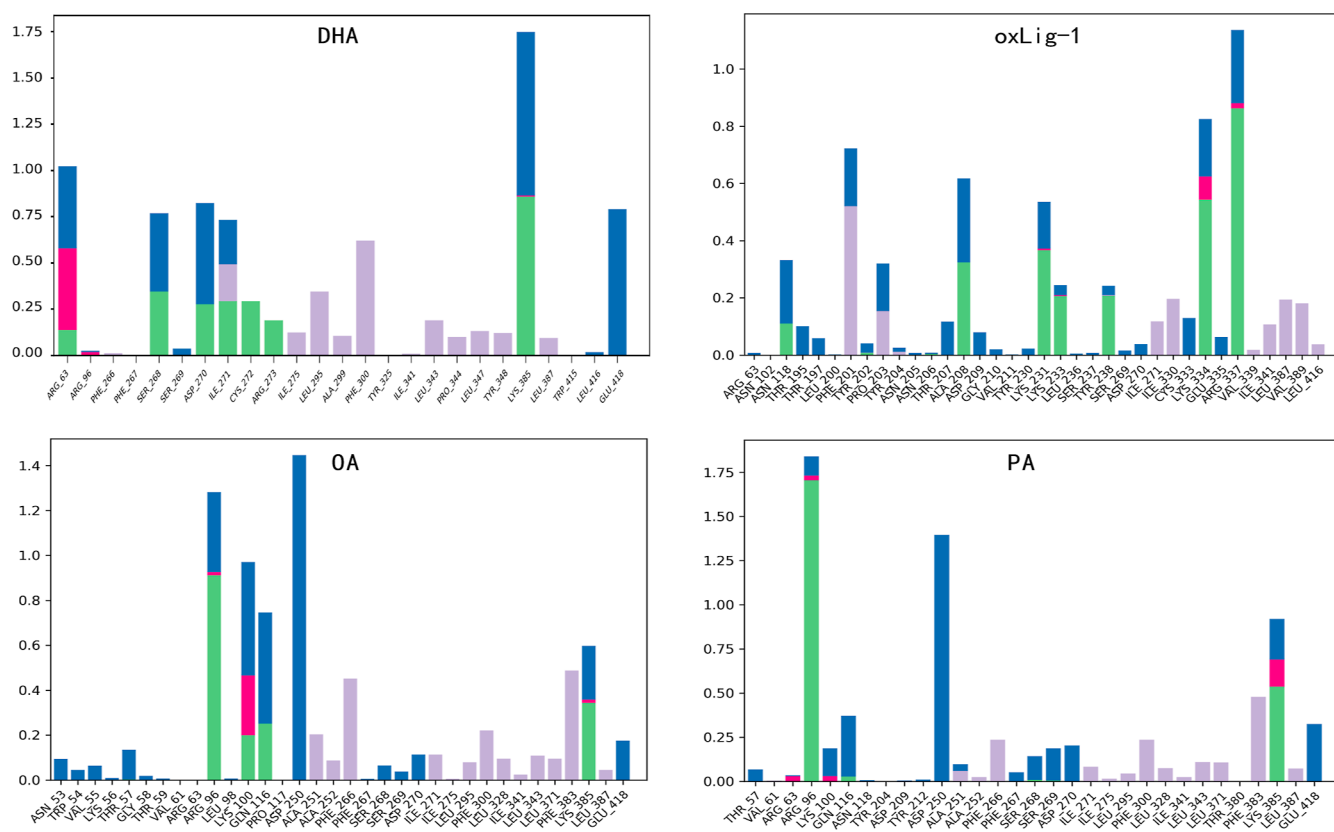
Figure 6. Interactions of complex that the CD36 grid3 bind with selected compounds monitored throughout the simulation trajectories. Interaction types: hydrogen bonds (green), hydrophobic (light purple), ionic (pink), and water bridges (blue).
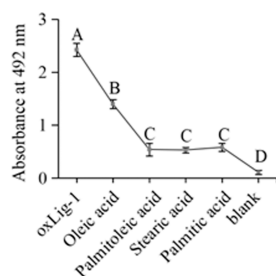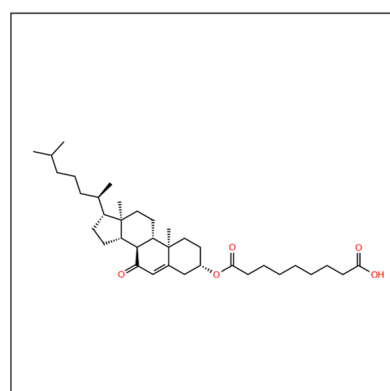

Figure 7. Binding activity of oxLig-1, oleic acid, palmitoleic acid, stearic acid, and palmitic acid to CD36. Data are presented as mean $\pm$ SD ($n =$ 3), [A,B,C,D] means with different superscripts are significantly different ($p < 0.01$).

LCFAs, thus providing a possibility for the treatment of lipid metabolism disorders.

In the molecular docking operations, LCFAs bound to the three predicted potential binding sites (Grid1−3) of CD36. OxLig-1 bound to Grid3 of the protein. The main driving force for ligand and protein binding was hydrophobic and intermolecular hydrogen bonding. Depending on the saturation and chain length, unsaturated LCFAs as well as oxLig-1 may have a better binding ability to proteins than other fatty acids, perhaps due to the 3D spatial structure of fatty acid chains containing more carbon−carbon double bonds being better adapted to the hydrophobic cavities of proteins.[60] Since oxLig-1 contains a cholesterol parent nucleus, this creates a spatial barrier at the molecular level that prevented it from entering
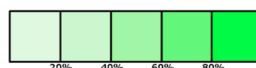

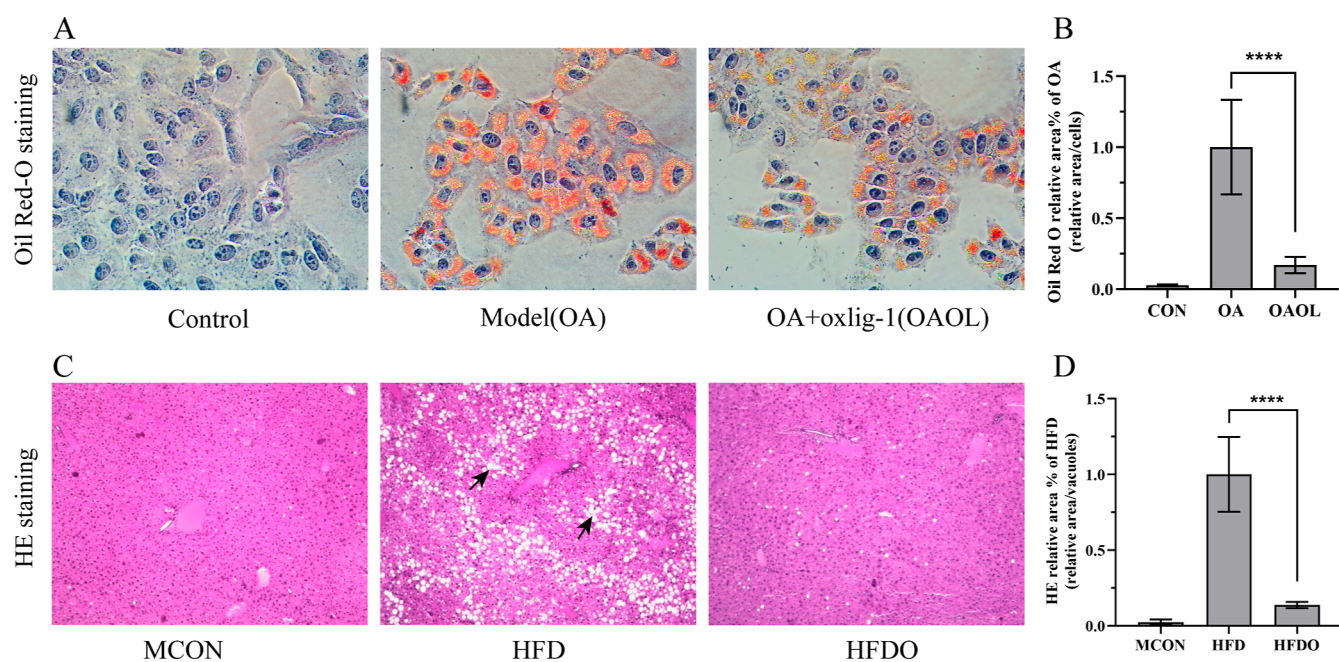**Figure 8.** Toxicity evaluation of oxLig-1.

Figure 9. OxLig-1 intervention reduces lipid deposition. (A) OxLig-1 intervention reduces lipid deposition of HepG2 cells induced by oleic acid (magnification ×400). (B) Ratio of Oil Red-O-stained area to cell number (n = 6 cell images/group). (C) OxLig-1 decreases liver lipid deposition induced by HFD in mice (magnification ×100). (D) Ratio of lipid vacuoles (black arrowheads) area to histological section area (n = 10 histological images/group). All data are presented as the mean ± SD, ****p < 0.0001.

CD36 Grid1 or Grid2 and it bound better to a common "lumen" formed by the convergence of the ends of Grid1 and Grid2, which was another protein binding pocket that we obtained by calculating the protein potential binding sites, labeled Grid3, in which oxLig-1 had a better affinity than some other LCFAs. This work also examined the role of CD36 protein uptake into cell by binding LCFAs and molecules, such as oxLig-1. For the process of entry of molecules such as LCFAs into the cell after binding to CD36, the study by Hao et al. found that CD36 promoted intracellular transport of fatty acids through dynamics palmitoylation-regulated cellular internalization.[61] There may be other mechanisms regulating the role of proteins entering the cell after binding to LCFAs,[62] as well as the role of dissociation from the protein binding pocket after entry, that need to be further explored.

During the MD simulation, the binding trajectory started to change after entering the solvent system, the complex system gradually converged after a certain time and the atomic changes of the ligand and receptor decreased.[63] The overall ligand rmsd of oxLig-1 was significantly less than that of DHA and PA, which may indicate that oxLig-1 and CD36 may have more stable binding effects during the binding kinetics of ligand molecules to receptor proteins. It did not fluctuate as much as that of oleic acid. The long chain of the azelaic acid group in the oxLig-1 molecule was free at the opening of the binding pocket, forming a fluctuation of the carbon chain backbone within the molecule, which is the main source of change in the rmsd of the ligand. In turn, the carboxyl group at the end of the azelaic acid formed hydrogen bonds dynamically with the amino acid residues of the protein molecule,[64] thus stabilizing the complex.

Furthermore, when the complex with oxLig-1 docked to CD36 was subjected to potential site calculations a second time, the computational task failed, pointing to conflicting atomic positions. This implies that oxLig-1 may play a role in inhibiting the binding of LCFAs to CD36 by occupying the "confluent"

part of the natural channel within the CD36 molecule and binding stably to it, thereby reducing the uptake of LCFAs by cells via the major lipid receptor CD36. OxLig-1 may play a role in inhibiting binding of LCFAs to CD36, reducing the uptake of LCFAs by cells through the major lipid receptor CD36. In contrast, DHA and other polyunsaturated LCFAs have a high affinity for proteins, and it is assumed that oxLig-1 may not have an inhibitory effect on their uptake.

The ADMET properties of potential drug candidates are important for their efficacy and safety as therapeutics.[65] ADMET predictions indicated that the absorption of compound oxLig-1 was expected to be good. For its distribution, plasma protein binding was high and the volume distribution was within the optimal range. In terms of metabolism, oxLig-1 did not inhibit most cytochromes. Excretion of oxLig-1 was a moderate rate, and toxicity was in the low toxicity range. These parameters were checked to be within their standard ranges and suggested that oxLig-1 is suitable for further development as a lead compound.

In NAFLD patients, the uptake of circulating lipids, in particular LCFAs by the liver is increased, the excessive LCFAs influx to hepatocytes is the earliest event triggering lipotoxicity. This increased uptake is related to the enhanced level of lipid transport proteins in the plasma membrane.[66] To better clear circulating fatty acids, the liver upregulates expression of the hepatic fatty acid transporter CD36; it is well known that CD36 increases LCFAs uptake and, in the hepatocytes, it drives hepatic steatosis onset and might contribute to its progression to nonalcoholic steatohepatitis (NASH).[67] In this study, molecular docking and MD simulations of oxlig-1 and different types of LCFAs with CD36 receptors showed a trend that the molecular binding ability and binding stability of LCFAs decreased from polyunsaturated LCFAs, oxLig-1, monounsaturated LCFAs to saturated LCFAs. ELISA results also showed that the binding activity of oxLig-1 to CD36 was significantly higher than that of

monounsaturated (oleic acid and palmitoleic acid) and saturated fatty acids (stearic acid and palmitic acid), oxLig-1 played an important lipid-lowering role in HepG2 cells model of oleic acid and NAFLD mice model. Combined with our previous findings that oxLig-1 can induce CD36-dependent activation of JNK/ABCA1 and PPAR/ABCA1 signaling pathways.[34,35] Taken together, these results strongly suggest that oxLig-1 may have a protective role in inhibiting hepatocyte lipid deposition in lipotoxicy monounsaturated and saturated LCFAs by targeting CD36. The mechanism of its action as a drug deserves further investigation.

■ AUTHOR INFORMATION

Corresponding Authors

Mingzhi Zhang — *Joint Shantou International Eye Center of Shantou University and The Chinese University of Hong Kong, Shantou, Guangdong Province 515041, China*; Email: zmz@jsiec.org

Qingping Liu — *Joint Shantou International Eye Center of Shantou University and The Chinese University of Hong Kong, Shantou, Guangdong Province 515041, China; Key Laboratory of Carbohydrate and Lipid Metabolism Research of Liaoning Province, Dalian, Liaoning Province 116024, China*; Email: qingpingliu40@hotmail.com

Authors

Changzhen Fu — *Joint Shantou International Eye Center of Shantou University and The Chinese University of Hong Kong, Shantou, Guangdong Province 515041, China*

Meng-Lin Xiang — *Joint Shantou International Eye Center of Shantou University and The Chinese University of Hong Kong, Shantou, Guangdong Province 515041, China; Shantou University Medical College, Shantou, Guangdong Province 515031, China;* orcid.org/0000-0002-0399-0770

Shaolang Chen — *Joint Shantou International Eye Center of Shantou University and The Chinese University of Hong Kong, Shantou, Guangdong Province 515041, China*

Geng Dong — *Shantou University Medical College, Shantou, Guangdong Province 515031, China*

Zibo Liu — *Joint Shantou International Eye Center of Shantou University and The Chinese University of Hong Kong, Shantou, Guangdong Province 515041, China;* orcid.org/0000-0002-5363-3819

Chong-Bo Chen — *Joint Shantou International Eye Center of Shantou University and The Chinese University of Hong Kong, Shantou, Guangdong Province 515041, China*

Jiajian Liang — *Joint Shantou International Eye Center of Shantou University and The Chinese University of Hong Kong, Shantou, Guangdong Province 515041, China*

Yingjie Cao — *Joint Shantou International Eye Center of Shantou University and The Chinese University of Hong Kong, Shantou, Guangdong Province 515041, China*

Complete contact information is available at:
https://pubs.acs.org/10.1021/acsomega.3c02082

Author Contributions

‖C.F. and M.-L.X. contributed equally to this work.

Notes

The authors declare no competing financial interest.

■ REFERENCES

(1) Younossi, Z. M.; Golabi, P.; Paik, J. M.; Henry, A.; Van Dongen, C.; Henry, L. The global epidemiology of nonalcoholic fatty liver disease (NAFLD) and nonalcoholic steatohepatitis (NASH): a systematic review. *Hepatology* **2023**, *77*, 1335−1347.

(2) Pugliese, N.; Alfarone, L.; Arcari, I.; Giugliano, S.; Parigi, T. L.; Rescigno, M.; Lleo, A.; Aghemo, A. Clinical features and management issues of NAFLD-related HCC: what we know so far. *Expert Rev. Gastroenterol. Hepatol.* **2023**, *17*, 31−43.

(3) Foerster, F.; Gairing, S. J.; Müller, L.; Galle, P. R. NAFLD-driven HCC: Safety and efficacy of current and emerging treatment options. *J. Hepatol.* **2022**, *76*, 446−457.

(4) Ioannou, G. N. Epidemiology and risk-stratification of NAFLD-associated HCC. *J. Hepatol.* **2021**, *75*, 1476−1484.

(5) Do, M. H.; Lee, H. H. L.; Lee, J. E.; Park, M.; Oh, M. J.; Lee, H. B.; Park, J. H.; Jhun, H.; Kim, J. H.; Kang, C. H.; et al. Gellan gum prevents non-alcoholic fatty liver disease by modulating the gut microbiota and metabolites. *Food Chem.* **2023**, *400*, 134038.

(6) Shen, K.; Singh, A. D.; Modaresi Esfeh, J.; Wakim-Fleming, J. Therapies for non-alcoholic fatty liver disease: A 2022 update. *World J. Hepatol.* **2022**, *14*, 1718−1729.

(7) Xu, X.; Poulsen, K. L.; Wu, L.; Liu, S.; Miyata, T.; Song, Q.; Wei, Q.; Zhao, C.; Lin, C.; Yang, J. Targeted therapeutics and novel signaling pathways in non-alcohol-associated fatty liver/steatohepatitis (NAFL/NASH). *Signal Transduction Targeted Ther.* **2022**, *7*, 287.

(8) Su, X.; Abumrad, N. A. Cellular fatty acid uptake: a pathway under construction. *Trends Endocrinol. Metab.* **2009**, *20*, 72−77.

(9) Samovski, D.; Jacome-Sosa, M.; Abumrad, N. A. Fatty Acid Transport and Signaling: Mechanisms and Physiological Implications. *Annu. Rev. Physiol.* **2023**, *85*, 317−337.

(10) Pepino, M. Y.; Kuda, O.; Samovski, D.; Abumrad, N. A. Structure-function of CD36 and importance of fatty acid signal transduction in fat metabolism. *Annu. Rev. Nutr.* **2014**, *34*, 281−303.

(11) Tsuzuki, S.; Yamasaki, M.; Kozai, Y.; Sugawara, T.; Manabe, Y.; Inoue, K.; Fushiki, T. Assessment of direct interaction between CD36 and an oxidized glycerophospholipid species. *J. Biochem.* **2017**, *162*, 163−172.

(12) Clemetson, K. J.; Pfueller, S. L.; Luscher, E. F.; Jenkins, C. S. Isolation of the membrane glycoproteins of human blood platelets by lectin affinity chromatography. *Biochim. Biophys. Acta* **1977**, *464*, 493−508.

(13) Knowles, D. M., 2nd; Tolidjian, B.; Marboe, C.; D'Agati, V.; Grimes, M.; Chess, L. Monoclonal anti-human monocyte antibodies OKM1 and OKM5 possess distinctive tissue distributions including differential reactivity with vascular endothelium. *J. Immunol.* **1984**, *132*, 2170−2173.

(14) Abumrad, N. A.; el-Maghrabi, M. R.; Amri, E. Z.; Lopez, E.; Grimaldi, P. Cloning of a rat adipocyte membrane protein implicated in binding or transport of long-chain fatty acids that is induced during preadipocyte differentiation. Homology with human CD36. *J. Biol. Chem.* **1993**, *268*, 17665−17668.

(15) Endemann, G.; Stanton, L. W.; Madden, K. S.; Bryant, C.; White, R.; Protter, A. CD36 is a receptor for oxidized low density lipoprotein. *J. Biol. Chem.* **1993**, *268*, 11811−11816.

(16) Hsieh, F. L.; Turner, L.; Bolla, J. R.; Robinson, C. V.; Lavstsen, T.; Higgins, M. K. The structural basis for CD36 binding by the malaria parasite. *Nat. Commun.* **2016**, *7*, 12837.

(17) Glatz, J. F. C.; Luiken, J. Dynamic role of the transmembrane glycoprotein CD36 (SR-B2) in cellular fatty acid uptake and utilization. *J. Lipid Res.* **2018**, *59*, 1084−1093.

(18) Olzmann, J. A.; Carvalho, P. Dynamics and functions of lipid droplets. *Nat. Rev. Mol. Cell Biol.* **2019**, *20*, 137−155.

(19) Kopchick, J. J.; Berryman, D. E.; Puri, V.; Lee, K. Y.; Jorgensen, J. O. L. The effects of growth hormone on adipose tissue: old observations, new mechanisms. *Nat. Rev. Endocrinol.* **2020**, *16*, 135−146.

(20) Liu, Y.; Charpin-El Hamri, G.; Ye, H.; Fussenegger, M. A synthetic free fatty acid-regulated transgene switch in mammalian cells and mice. *Nucleic Acids Res.* **2018**, *46*, 9864−9874.

(21) Piccolis, M.; Bond, L. M.; Kampmann, M.; Pulimeno, P.; Chitraju, C.; Jayson, C. B.; Vaites, L. P.; Boland, S.; Lai, Z. W.; Gabriel, K. R.; et al. Probing the Global Cellular Responses to Lipotoxicity Caused by Saturated Fatty Acids. *Mol. Cell* **2019**, *74*, 32−44.e8.

(22) Saini, R. K.; Keum, Y. S. Omega-3 and omega-6 polyunsaturated fatty acids: Dietary sources, metabolism, and significance - A review. *Life Sci.* **2018**, *203*, 255−267.

(23) Briggs, M. A.; Petersen, K. S.; Kris-Etherton, P. M. Saturated Fatty Acids and Cardiovascular Disease: Replacements for Saturated Fat to Reduce Cardiovascular Risk. *Healthcare (Basel, Switzerland)* **2017**, *5*, 29.

(24) Basson, A. R.; Chen, C.; Sagl, F.; Trotter, A.; Bederman, I.; Gomez-Nguyen, A.; Sundrud, M. S.; Ilic, S.; Cominelli, F.; Rodriguez-Palacios, A. Regulation of Intestinal Inflammation by Dietary Fats. *Front. Immunol.* **2021**, *11*, 604989.

(25) Lee, D. H.; Park, J. S.; Lee, Y. S.; Han, J.; Lee, D. K.; Kwon, S. W.; Han, D. H.; Lee, Y. H.; Bae, S. H. SQSTM1/p62 activates NFE2L2/NRF2 via ULK1-mediated autophagic KEAP1 degradation and protects mouse liver from lipotoxicity. *Autophagy* **2020**, *16*, 1949−1973.

(26) Czumaj, A.; Śledziński, T. Biological Role of Unsaturated Fatty Acid Desaturases in Health and Disease. *Nutrients* **2020**, *12*, 356.

(27) Das, U. N. Essential fatty acids: biochemistry, physiology and pathology. *Biotechnol. J.* **2006**, *1*, 420−439.

(28) Scorletti, E.; Byrne, C. D. Omega-3 fatty acids and non-alcoholic fatty liver disease: Evidence of efficacy and mechanism of action. *Mol. Aspects Med.* **2018**, *64*, 135−146.

(29) Donnelly, K. L.; Smith, C. I.; Schwarzenberg, S. J.; Jessurun, J.; Boldt, M. D.; Parks, E. J. Sources of fatty acids stored in liver and secreted via lipoproteins in patients with nonalcoholic fatty liver disease. *J. Clin. Invest.* **2005**, *115*, 1343−1351.

(30) Lei, S. S.; Zhang, N. Y.; Zhou, F. C.; He, X.; Wang, H. Y.; Li, L. Z.; Zheng, X.; Dong, Y. J.; Luo, R.; Li, B.; et al. Dendrobium officinale Regulates Fatty Acid Metabolism to Ameliorate Liver Lipid Accumulation in NAFLD Mice. *Evidence-Based Complementary Altern. Med.* **2021**, *2021*, 6689727.

(31) Dong, Y.; Lu, H.; Li, Q.; Qi, X.; Li, Y.; Zhang, Z.; Chen, J.; Ren, J. (5R)-5-hydroxytriptolide ameliorates liver lipid accumulation by suppressing lipid synthesis and promoting lipid oxidation in mice. *Life Sci.* **2019**, *232*, 116644.

(32) Kobayashi, K.; Matsuura, E.; Liu, Q.; Furukawa, J. i.; Kaihara, K.; Inagaki, J.; Atsumi, T.; Sakairi, N.; Yasuda, T.; Voelker, D. R.; et al. A specific ligand for β2-glycoprotein I mediates autoantibody-dependent uptake of oxidized low density lipoprotein by macrophages. *J. Lipid Res.* **2001**, *42*, 697−709.

(33) Liu, Q.; Kobayashi, K.; Furukawa, J.; Inagaki, J.; Sakairi, N.; Iwado, A.; Yasuda, T.; Koike, T.; Voelker, D. R.; Matsuura, E. ω-Carboxyl variants of 7-ketocholesteryl esters are ligands for β2-glycoprotein I and mediate antibody-dependent uptake of oxidized LDL by macrophages. *J. Lipid Res.* **2002**, *43*, 1486−1495.

(34) Li, W.; Wang, D.; Chi, Y.; Wang, R.; Zhang, F.; Ma, G.; Chen, Z.; Li, J.; Liu, Z.; Matsuura, E.; et al. 7-Ketocholesteryl-9-carboxynonanoate enhances the expression of ATP-binding cassette transporter A1 via CD36. *Atherosclerosis* **2013**, *226*, 102−109.

(35) Li, J.; Xiu, Z.; Wang, R.; Yu, C.; Chi, Y.; Qin, J.; Fu, C.; Matsuura, E.; Liu, Q. The lipid moiety 7-ketocholesteryl-9-carboxynonanoate mediates binding interaction of oxLDL to LOX-1 and upregulates ABCA1 expression through PPARγ. *Life Sci.* **2017**, *177*, 27−40.

(36) Li, J.; Yu, C.; Wang, R.; Xu, J.; Chi, Y.; Qin, J.; Liu, Q. The omega-carboxyl group of 7-ketocholesteryl-9-carboxynonanoate mediates the

binding of oxLDL to CD36 receptor and enhances caveolin-1 expression in macrophages. *Int. J. Biochem. Cell Biol.* **2017**, *90*, 121−135.

(37) Dhiman, A.; Purohit, R. Identification of potential mutational hotspots in serratiopeptidase to address its poor pH tolerance issue. *J. Biomol. Struct. Dyn.* **2022**, 1−13.

(38) Kumar, S.; Bhardwaj, V. K.; Singh, R.; Purohit, R. Structure restoration and aggregate inhibition of V30M mutant transthyretin protein by potential quinoline molecules. *Int. J. Biol. Macromol.* **2023**, *231*, 123318.

(39) Singh, R.; Bhardwaj, V.; Purohit, R. Identification of a novel binding mechanism of Quinoline based molecules with lactate dehydrogenase of Plasmodium falciparum. *J. Biomol. Struct. Dyn.* **2021**, *39*, 348−356.

(40) Pirolli, D.; Righino, B.; Camponeschi, C.; Ria, F.; Di Sante, G.; De Rosa, M. C. Virtual screening and molecular dynamics simulations provide insight into repurposing drugs against SARS-CoV-2 variants Spike protein/ACE2 interface. *Sci. Rep.* **2023**, *13*, 1494.

(41) Bhardwaj, V. K.; Purohit, R. Targeting the protein-protein interface pocket of Aurora-A-TPX2 complex: rational drug design and validation. *J. Biomol. Struct. Dyn.* **2021**, *39*, 3882−3891.

(42) Tuccinardi, T. What is the current value of MM/PBSA and MM/GBSA methods in drug discovery? *Expert Opin. Drug Discov.* **2021**, *16*, 1233−1237.

(43) Genheden, S.; Ryde, U. The MM/PBSA and MM/GBSA methods to estimate ligand-binding affinities. *Expert Opin. Drug Discov.* **2015**, *10*, 449−461.

(44) Wang, E.; Sun, H.; Wang, J.; Wang, Z.; Liu, H.; Zhang, J. Z. H.; Hou, T. End-Point Binding Free Energy Calculation with MM/PBSA and MM/GBSA: Strategies and Applications in Drug Design. *Chem. Rev.* **2019**, *119*, 9478−9508.

(45) Tian, K.; Xu, Y.; Sahebkar, A.; Xu, S. CD36 in Atherosclerosis: Pathophysiological Mechanisms and Therapeutic Implications. *Curr. Atheroscler. Rep.* **2020**, *22*, 59.

(46) Vazquez, M. M.; Gutierrez, M. V.; Salvatore, S. R.; Puiatti, M.; Dato, V. A.; Chiabrando, G. A.; Freeman, B. A.; Schopfer, F. J.; Bonacci, G. Nitro-oleic acid, a ligand of CD36, reduces cholesterol accumulation by modulating oxidized-LDL uptake and cholesterol efflux in RAW264.7 macrophages. *Redox Biol.* **2020**, *36*, 101591.

(47) Yang, R.; Liu, Q.; Zhang, M. The Past and Present Lives of the Intraocular Transmembrane Protein CD36. *Cells* **2022**, *12*, 171.

(48) Daquinag, A. C.; Gao, Z.; Fussell, C.; Immaraj, L.; Pasqualini, R.; Arap, W.; Akimzhanov, A. M.; Febbraio, M.; Kolonin, M. G. Fatty acid mobilization from adipose tissue is mediated by CD36 posttranslational modifications and intracellular trafficking. *JCI Insight* **2021**, *6*, No. e147057.

(49) Pantsar, T.; Kaiser, P. D.; Kudolo, M.; Forster, M.; Rothbauer, U.; Laufer, S. A. Decisive role of water and protein dynamics in residence time of p38α MAP kinase inhibitors. *Nat. Commun.* **2022**, *13*, 569.

(50) Mark, P.; Nilsson, L. Structure and Dynamics of the TIP3P, SPC, and SPC/E Water Models at 298 K. *J. Phys. Chem. A* **2001**, *105*, 9954−9960.

(51) Essmann, U.; Perera, L.; Berkowitz, M. L.; Darden, T.; Lee, H.; Pedersen, L. G. A smooth particle mesh Ewald method. *J. Chem. Phys.* **1995**, *103*, 8577−8593.

(52) Ebrahimi, M.; Karami, L.; Alijanianzadeh, M. Computational repurposing approach for targeting the critical spike mutations in B.1.617.2 (delta), AY.1 (delta plus) and C.37 (lambda) SARS-CoV-2 variants using exhaustive structure-based virtual screening, molecular dynamic simulations and MM-PBSA methods. *Comput. Biol. Med.* **2022**, *147*, 105709.

(53) Huang, Z.; Li, W.; Wang, R.; Zhang, F.; Chi, Y.; Wang, D.; Liu, Z.; Zhang, Y.; Matsuura, E.; Liu, Q. 7-ketocholesteryl-9-carboxynonanoate induced nuclear factor-kappa B activation in J774A.1 macrophages. *Life Sci.* **2010**, *87*, 651−657.

(54) Xiong, G.; Wu, Z.; Yi, J.; Fu, L.; Yang, Z.; Hsieh, C.; Yin, M.; Zeng, X.; Wu, C.; Lu, A.; et al. ADMETlab 2.0: an integrated online

platform for accurate and comprehensive predictions of ADMET properties. *Nucleic Acids Res.* **2021**, *49*, W5−w14.

(55) Banerjee, P.; Eckert, A. O.; Schrey, A. K.; Preissner, R. ProTox-II: a webserver for the prediction of toxicity of chemicals. *Nucleic Acids Res.* **2018**, *46*, W257−w263.

(56) Meli, R.; Biggin, P. C. , spyrmsd: symmetry-corrected RMSD calculations in Python. *J. Cheminform.* **2020**, *12*, 49.

(57) van Breemen, R. B.; Li, Y. Caco-2 cell permeability assays to measure drug absorption. *Expert Opin. Drug Metab. Toxicol.* **2005**, *1*, 175−185.

(58) Lian, C. Y.; Zhai, Z. Z.; Li, Z. F.; Wang, L. High fat diet-triggered non-alcoholic fatty liver disease: A review of proposed mechanisms. *Chem. Biol. Interact.* **2020**, *330*, 109199.

(59) Katsiki, N.; Stoian, A. P.; Rizzo, M. Dietary patterns in non-alcoholic fatty liver disease (NAFLD): Stay on the straight and narrow path. *Clin. Investig. Arterioscler.* **2022**, *34*, S24−S31.

(60) Deeken, R.; Saupe, S.; Klinkenberg, J.; Riedel, M.; Leide, J.; Hedrich, R.; Mueller, T. D. The Nonspecific Lipid Transfer Protein AtLtpI-4 Is Involved in Suberin Formation of Arabidopsis thaliana Crown Galls. *Plant Physiol.* **2016**, *172*, 1911−1927.

(61) Hao, J. W.; Wang, J.; Guo, H.; Zhao, Y. Y.; Sun, H. H.; Li, Y. F.; Lai, X. Y.; Zhao, N.; Wang, X.; Xie, C.; et al. CD36 facilitates fatty acid uptake by dynamic palmitoylation-regulated endocytosis. *Nat. Commun.* **2020**, *11*, 4765.

(62) Field, C. S.; Baixauli, F.; Kyle, R. L.; Puleston, D. J.; Cameron, A. M.; Sanin, D. E.; Hippen, K. L.; Loschi, M.; Thangavelu, G.; Corrado, M.; et al. Mitochondrial Integrity Regulated by Lipid Metabolism Is a Cell-Intrinsic Checkpoint for Treg Suppressive Function. *Cell Metab.* **2020**, *31*, 422−437.

(63) Chen, J.; Haller, C. A.; Jernigan, F. E.; Koerner, S. K.; Wong, D. J.; Wang, Y.; Cheong, J. E.; Kosaraju, R.; Kwan, J.; Park, D. D.; et al. Modulation of lymphocyte-mediated tissue repair by rational design of heterocyclic aryl hydrocarbon receptor agonists. *Sci. Adv.* **2020**, *6*, No. eaay8230.

(64) Kostrzewa, T.; Sahu, K. K.; Gorska-Ponikowska, M.; Tuszynski, J. A.; Kuban-Jankowska, A. Synthesis of small peptide compounds, molecular docking, and inhibitory activity evaluation against phosphatases PTP1B and SHP2. *Drug Des., Dev. Ther.* **2018**, *12*, 4139−4147.

(65) Feinberg, E. N.; Joshi, E.; Pande, V. S.; Cheng, A. C. Improvement in ADMET Prediction with Multitask Deep Featurization. *J. Med. Chem.* **2020**, *63*, 8835−8848.

(66) Geisler, C. E.; Renquist, B. J. Hepatic lipid accumulation: cause and consequence of dysregulated glucoregulatory hormones. *J. Endocrinol.* **2017**, *234*, R1−R21.

(67) Rada, P.; González-Rodríguez, Á.; García-Monzón, C.; Valverde, A. M. Understanding lipotoxicity in NAFLD pathogenesis: is CD36 a key driver? *Cell Death Dis.* **2020**, *11*, 802.